Available online at www.sciencedirect.com
ScienceDirect
Radiation Measurements 41 (2006) 1080–1090
Radiation Measurements
www.elsevier.com/locate/radmeas

PHITS—a particle and heavy ion transport code system

Koji Niita[a,*], Tatsuhiko Sato[b], Hiroshi Iwase[c], Hiroyuki Nose[d], Hiroshi Nakashima[b], Lembit Sihver[e,f]

[a]*Research Organization for Information Science & Technology (RIST), 2-4 Shirane, Shirakata, Tokai, Naka, Ibaraki 319-1106, Japan*
[b]*Japan Atomic Energy Research Institute (JAERI), Japan*
[c]*GSI, Germany*
[d]*Ishikawajima-Harima Heavy Industries Co., Ltd. (IHI), Japan*
[e]*Chalmers University of Technology, Sweden*
[f]*Roanoke College, USA*

Received 11 May 2005; received in revised form 7 April 2006; accepted 2 July 2006

Abstract

The paper presents a summary of the recent development of the multi-purpose Monte Carlo Particle and Heavy Ion Transport code System, PHITS. In particular, we discuss in detail the development of two new models, JAM and JQMD, for high energy particle interactions, incorporated in PHITS, and show comparisons between model calculations and experiments for the validations of these models. The paper presents three applications of the code including spallation neutron source, heavy ion therapy and space radiation. The results and examples shown indicate PHITS has great ability of carrying out the radiation transport analysis of almost all particles including heavy ions within a wide energy range.

1. Introduction

Particle and heavy ion transport code is an essential implement in design and study of spacecrafts and accelerator facilities. We have therefore developed the multi-purpose Monte Carlo Particle and Heavy Ion Transport code System, PHITS (Iwase et al., 2002), based on the NMTC/JAM (Niita et al., 2001).

The physical processes which we should deal with in a multi-purpose simulation code can be divided into two categories, transport process and collision process. In the transport process, PHITS can simulate a motion under external fields such as magnetic and gravity. Without the external fields, neutral particles move along a straight trajectory with constant energy up to the next collision point. However, charge particles and heavy ions interact many times with electrons in the material losing energy and changing direction. PHITS treats ionization processes not as collision but as a transport process under an external field. The average dE/dx is given by the charge density of the material and the momentum of the particle taking into account the fluctuations of the energy loss and the angular deviation.

The second category of the physical processes is the collision with the nucleus in the material. In addition to the collision, we consider the decay of the particle as a process in this category. The total reaction cross section, or the life time of the particle is an essential quantity in the determination of the mean free path of the transport particle. According to the mean free path, PHITS chooses the next collision point using the Monte Carlo method. To generate the secondary particles of the collision, we need the information of the final states of the collision. For neutron induced reactions in low energy region, PHITS employs the cross sections from Evaluated Nuclear Data libraries such as ENDF-B/VI (McLane et al., 1996) and JENDL-3.3 library (Shibata et al., 2002) up to 20 MeV and LA150 up to 150 MeV (Chadwick et al., 1999). PHITS also uses Evaluated Nuclear Data for photon and electron transport below 1 GeV in the same manner as in the MCNP4C code (Briesmeister et al., 1997) based on ITS version 3.0 code (Halbleib et al., 1992). For high energy neutrons and other particles, we have incorporated two new models, JAM (Nara et al., 2000) and JQMD

* Corresponding author. Tel.: +81 29 282 5017; fax: +81 29 287 0315.
E-mail address: niita@tokai.rist.or.jp (K. Niita).

1350-4487/$ - see front matter © 2006 Elsevier Ltd. All rights reserved.
doi:10.1016/j.radmeas.2006.07.013

(Niita et al., 1995) to simulate the particle induced reactions up to 200 GeV and the nucleus–nucleus collisions, respectively. In this paper, we report the details of these models, and introduce some model applications.

2. 3D Monte Carlo method vs. deterministic approach

PHITS is a three-dimensional (3D) Monte Carlo transport code, which is frequently compared with the deterministic solution of the Boltzmann equation employed in HZETRN (Wilson et al., 1991). Before showing the details of the PHITS code, we first discuss these different approaches from a theoretical point of view. One could consider the 3D Monte Carlo approach as a numerical solution of the 3D Boltzmann equation by means of the test particle method where the one-body phase-space distribution function is evaluated by integrating the test particle tracks in the phase-space. In this sense, the physics described by both approaches are essentially the same as both methods use the same information of the cross sections. However, one could alternatively regard the 3D Monte Carlo approach as an event generator in which each collision is simulated keeping the energy and momentum conservation law. In this context, the two models are different. The solution of the Boltzmann equation includes only the mean values of the one-body observables in the phase space. It cannot give us the fluctuations around the mean value, since the Boltzmann equation has no information for the two-body and higher correlations which determine the fluctuation around the mean value of the one-body observables. On the other hand, the event generator keeps the higher correlations at each collision able to describe the fluctuations around the mean values of the one-body observables. A typical example for such a correlated quantity is the deposit energy distribution in a cell, which is necessary for the estimation of the response function of the detector or a single event upset probability of a semiconductor memory cell (soft error). The solution of the Boltzmann equation cannot describe the distribution but only the mean value. Furthermore, Monte Carlo calculations by using the nuclear data cannot deal with these quantities beyond the one-body observables, since the nuclear data includes only the inclusive one-body cross sections but no information of the correlations. For such observables, only an event generator which can keep higher correlations is an effective tool.

Apart from the correlation problem, the differences between the Monte Carlo method and the deterministic solution should be discussed from a technical point of view, i.e. the efficiency of the simulations. If one could know the detail of the physical situation of the problem before solving it, it is easy to set up the problem by restricting the phase space. In the simplest case, we can reduce the problem into a one-dimensional problem. In such a situation, the deterministic approach is very effective and suitable for an optimization study. However, for a case that we do not know which phase space contributes most to the point where the detector is set up, or the geometry of the problem is very complicated, we cannot set up any simple phase space to be solved in the deterministic approach. In these cases, we could learn a lot of things from the 3D Monte Carlo simulations. Since it is an impossible task to perform the 3D Monte Carlo simulation up to large enough statistics at every phase space point, we have to use 3D Monte Carlo simulation in an iterative way by making use of variance reduction techniques[1] to increase the statistics at the detector points keeping the initial geometry of the problem. In this manner, we might find a way to reduce the phase space to be solved in the deterministic approach, or we might obtain a good result with good statistics in the simulation. In addition, the 3D Monte Carlo simulation could play an important role in the final step of the optimization processes by using a realistic geometry and physical conditions. In this sense, the two approaches should be good complements to each other.

3. Main features of PHITS

In this section, we describe the main features of PHITS, the transport particles and their energy range, the magnetic field, the ionization process, the parameterization of total and elastic cross sections, and the basic models to simulate the nuclear reactions and showing some comparisons with the experimental data.

3.1. The transport particles and energy range

We first summarize the transport particles which we can deal with in the PHITS code and the energy range of them. We can transport neutrons from thermal energy up to 200 GeV. We have employed the same method as in the MCNP4C code for neutrons below 20 MeV down to 1 meV based on the Evaluated Nuclear Data, while we use the simulation model JAM above 20 MeV up to 200 GeV. For protons and other hadrons, we also use the simulation model JAM above 1 MeV up to 200 GeV, but we only consider the ionization process for charged particles below 1 MeV until they stop. PHITS can transport nucleus in the materials. Below 10 MeV/*u*, we only take into account the ionization process for the nucleus transport, but above 10 MeV/*u* we describe nucleus–nucleus collisions up to 100 GeV/*u* by the simulation model JQMD. As mentioned before, we have use the same method as in the MCNP4C code for electron and photon transport. Then the energy range of these particles is restricted within 1 keV and 1 GeV at the present. The extension of the maximum energy of these particles is now in progress.

3.2. The magnetic field

For simulating the transport of charge particles and heavy ions, the knowledge of the magnetic field is sometimes necessary to estimate beam loss, heat deposition in the magnet, and beam spread. PHITS can provide dipole and quadrupole magnetic fields in any direction and any region of the setup geometry. In contrast to other beam transport codes, PHITS can

[1] Some examples of the variance reduction techniques are explained in Briesmeister et al. (1997).

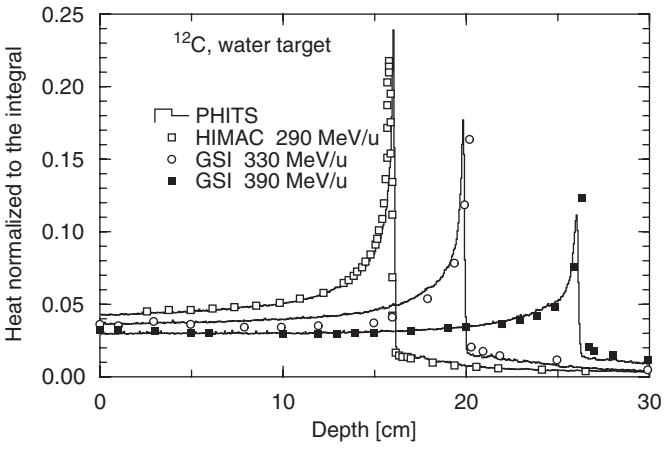

Fig. 1. Distribution of energy deposition as a function of depth along the axis of a cylindrical water target ($R = 10$ cm, $L = 30$ cm) irradiated with ^{12}C ion beams of 290, 330, and 390 MeV/u compared with the experimental data measured at HIMAC and GSI . Since the relative values were measured in the experiments, the value of heat is normalized as the integral values are coincident each other.

simulate not only the trajectory of the charge particles in the field, but also the collisions and the ionization process at the same time. This is a great advantage of PHITS for the design study of the high intensity proton and heavy ion accelerator facilities where one should estimate the radiation damage of the magnets and the surrounding materials and the shielding.

3.3. The ionization process

For the ionization process of the charge particles and nucleus, we have used the SPAR code (Armstrong and Chandler, 1973) for the average stopping power dE/dx, the first order of Moliere model for the angle straggling, and the Gaussian, Landau and Vavilov theories for the energy straggling around the average energy loss according to the charge density and velocity. Fig. 1 shows the distribution of energy deposition as a function of depth along the axis of the cylindrical water target ($R = 10$ cm, $L = 30$ cm) irradiated with ^{12}C ion beams of 290, 330, and 390 MeV/u compared with the experimental data measured at HIMAC of NIRS (Matsufuji et al., 2003) and GSI (Sihver et al., 1998). The results of PHITS reproduce quite well the data with respect not only to the Bragg peak, but also the contribution of the second particles produced by the nuclear reactions.

3.4. The total and elastic cross sections

It is important to use reliable data of total non-elastic and elastic cross sections for the particle and heavy ion transport even in the high energy region. Though the simulation models of nuclear reaction, the JAM and JQMD codes mentioned below, can predict the total non-elastic cross sections by simulation, the results do not always agree well with the experimental data. Even if the deviation from the experimental data is small in a reaction, this affects the flight length of the transport particle in the material very much. It is therefore better to normalize the differential cross sections obtained by the simulation models by the total non-elastic cross sections given by the Evaluated Nuclear Data (McLane et al., 1996; Shibata et al., 2002; Chadwick et al., 1999) or the systematics (Niita et al., 2001). We have used the Evaluated Nuclear Data for neutron induced reactions below 20 MeV, and the systematics above 20 MeV and for proton induced reactions of all energy range.

As for the elastic cross sections, the simulation models can calculate neither the total cross sections nor the double differential cross sections. We thus use the Evaluated Nuclear Data for neutron induced reactions below 20 MeV, and the systematics (Niita et al., 2001) above 20 MeV and for proton induced reactions of all energy range concerned with the total and also the double differential cross sections of elastic nucleon–nucleus reactions. It should be noted that PHITS does not yet include the elastic channel of nucleus–nucleus collisions, but this will be included in the near future.

Recently, we have adopted the NASA systematics (Tripathi et al., 1996, 1997, 1999) for the total nucleus–nucleus reaction cross sections, instead of the Shen formula (Wen-quinf et al., 1989). For the total cross section and angular distribution of elastic cross section of nucleon induced reactions, we have developed the systematics (Niita et al., 2001) based on the Pearlstein's systematics (Pearlstein, 1972, 1987, 1989). Fig. 2 shows the results for the systematics for the elastic cross section angular distributions. We compare the results with the experimental data (NEA Data Bank,) and LA150 (Chadwick et al., 1999). The parameterization results agree with the experimental data for all of the targets and the incident energies above 50 MeV up to 1 GeV.

3.5. JAM code

JAM (Jet AA Microscopic Transport Model) (Nara et al., 2000) is a hadronic cascade model, which explicitly treats all established hadronic states including resonances with explicit spin and isospin as well as their anti-particles. We have parameterized all hadron–hadron cross sections based on the resonance model and string model by fitting the available experimental data. Below the energy in the center-of-mass system (c.m.) $\sqrt{s} < 4$ GeV, the inelastic hadron–hadron collisions are described by the resonance formations and their decays, and at higher energies, string formation and their fragmentation into hadrons are assumed.

We have parameterized the resonance formation cross sections in terms of the extended Breit–Wigner form and used the established data (Particle-Data-Group, 2002) for its decay channels and probabilities. At an energy range above $\sqrt{s} > 4$–5 GeV, the (isolated) resonance picture breaks down because the width of the resonance becomes wider and the discrete levels get closer. The hadronic interactions at the energy range 4–5 $< \sqrt{s} <$ 10–100 GeV where it is characterized by the

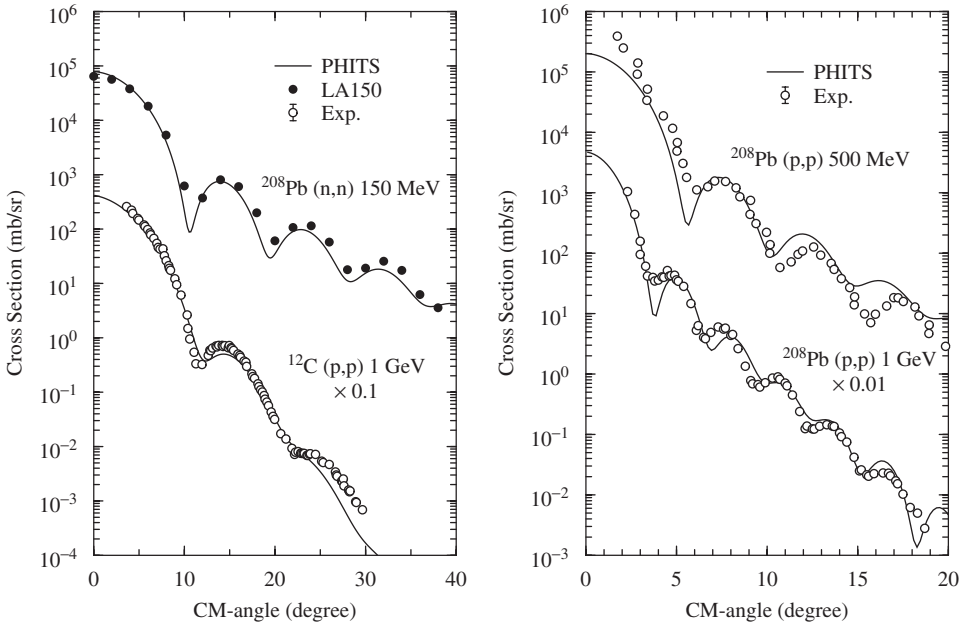

Fig. 2. Angular distribution of the elastic cross sections compared with the experimental data and LA150. The results of our systematic are denoted by solid lines.

small transverse momentum transfer is called "soft process", and string phenomenological models are known to describe the data for such soft interactions well. The hadron–hadron collision leads to a string-like excitation longitudinally. In the actual description of the string formation, we follow the prescription adopted in the HIJING model (Wang and Gyulassy, 1991, 1994; Wang, 1997). The strings are assumed to hadronize via quark-antiquark or diquark–antidiquark creation. As for the fragmentation of the strings, we adopted the Lund fragmentation model PYTHIA6.1 (Sjöstrand, 1994).

The detail of the parameterization of hadron–hadron cross sections in JAM is described in Nara et al. (2000). Here, we demonstrate a typical example of the elementary hadron–hadron cross sections obtained by JAM and compare results with the experimental data. In Fig. 3, we plot the total and elastic $\pi^- p$ and $K^+ p$ cross sections parameterized by JAM (upper panel), and the energy dependence of the exclusive cross sections of $K^- p \to \pi^0 \Lambda$ and $K^- n \to \pi^- \Sigma^0$(lower panel). Data are taken from (Particle-Data-Group, 2002; High Energy Reactions Analysis Group, 1983). It is recognized that JAM shows a good capability for calculating the cross sections even for the K, Λ, Σ.

For validation, we compare the results of JAM with experimental data of thin targets. In Fig. 4, we plot the invariant transverse mass distribution of proton (left panel) and π^+ (right panel) from protons on thin Au targets at 13.7 GeV. The results of JAM (histograms) and data (Tripathi et al., 1996, 1997, 1999) are plotted for each rapidity y bin quoted in the figure. For both ejectiles, the results of JAM agree well with the experimental data (Abbott et al., 1992). The agreement is also shown in the other targets of Be, Al, and Cu and the other ejectiles of π^- and K^+ in Nara et al. (2000).

3.6. JQMD code

The JQMD (JAERI Quantum Molecular Dynamics) code (Niita et al., 1995), has been widely used to analyze various aspects of heavy ion reactions as well as of nucleon-induced reactions (Chiba et al., 1996a,b). In the QMD model, the nucleus is described as a self-binding system of nucleons, which is interacting with each other through the effective interactions in the framework of molecular dynamics. One can estimate the yields of emitted light particles, fragments and of excited residual nuclei resulting from the heavy-ion collision. The QMD simulation, the JAM simulation as well, describes the dynamical stage of the reactions. At the end of the dynamical stage, we will get the excited nuclei from these simulations. To get the final observable, these excited nuclei should be decayed in a statistical way. We have employed GEM model (Furihata, 2000) (generalized evaporation model) for light particle evaporation and fission process of the excited residual nucleus.

So far the QMD model has shed light on several exciting topics in heavy-ion physics, for example, the multifragmentation, the flow of the nuclear matter, and the energetic particle productions (Aichelin, 1991). In Fig. 5 we show two examples of the basic observables from heavy-ion reactions calculated by the JQMD code. In Fig. 5(a) we represent the results of π^- energy spectra for the reaction $^{12}C+^{12}C$ at 800 MeV/u. The result of the JQMD code reproduces the experimental data (Tanihata et al., 1979). We notice that this calculation has been done in the same formulation and also with the same parameter set as used in the nucleon-induced reactions (Chiba et al., 1996a,b). Next example is the neutron energy spectra from the reaction $^{12}C+^{208}Pb$ at 400 MeV/u, which is shown in Fig. 5(b). The neutron produced in heavy-ion reactions is

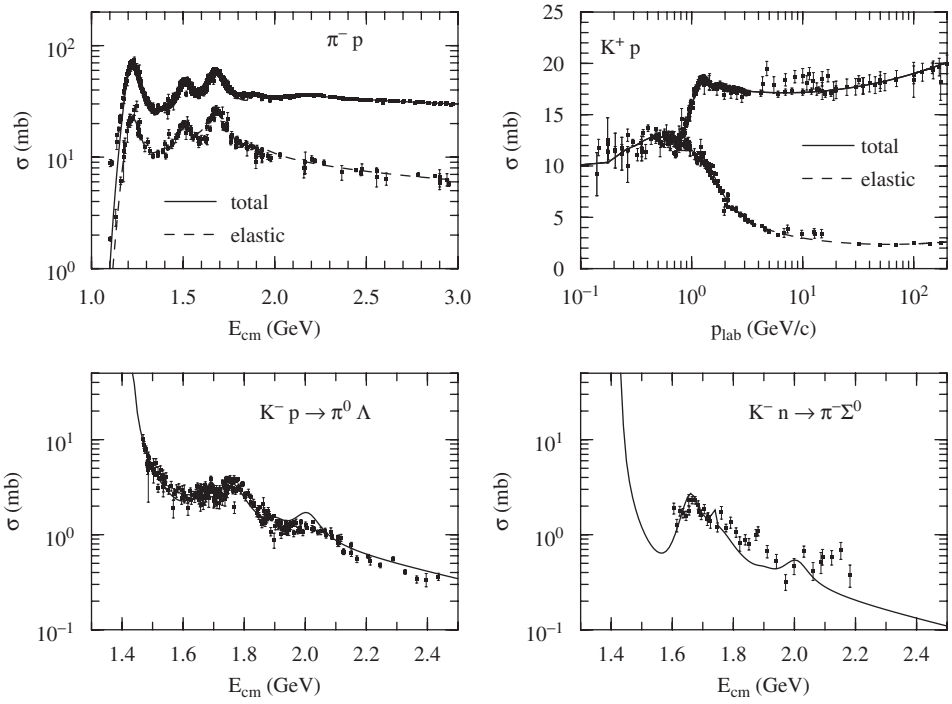

Fig. 3. Parameterization of the total and elastic $\pi^- p$ and $K^+ p$ cross sections (upper panel), and the energy dependence of the exclusive cross sections of $K^- p \to \pi^0 \Lambda$ and $K^- n \to \pi^- \Sigma^0$(lower panel). Data are taken from (Particle-Data-Group, 2002; High Energy Reactions Analysis Group, 1983).

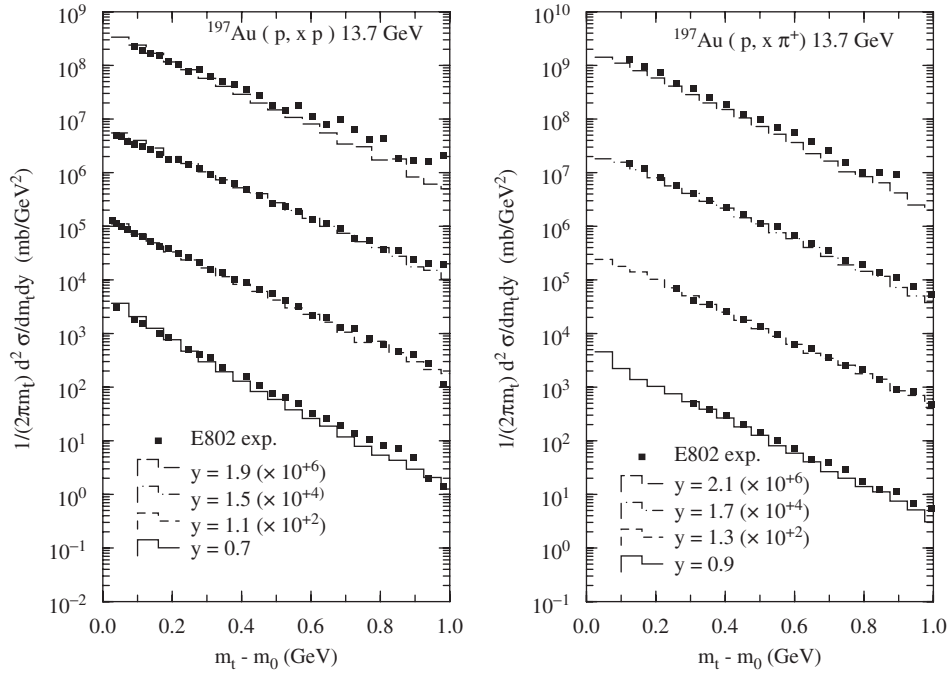

Fig. 4. Invariant transverse mass distribution of proton (left panel) and π^+ (right panel) from protons on thin Au targets at 13.7 GeV. The results of JAM (histograms) and data are plotted for each rapidity y bin quoted in the figure. In this figure, m_t is the transverse mass $\sqrt{p_x^2 + p_y^2 + m_0^2}$, where m_0 is the rest mass of proton, and the vertical axis denotes the Lorentz invariant double differential cross section.

very important in the shielding design of the spacecraft and the other facilities because of its large attenuation length in shielding materials. Recently, secondary neutrons from heavy-ion reactions have been systematically measured using thin and thick targets by HIMAC (Iwata et al., 2001; Kurosawa et al., 1999a–c, 2000). Fig. 5(b) shows that the JQMD code roughly

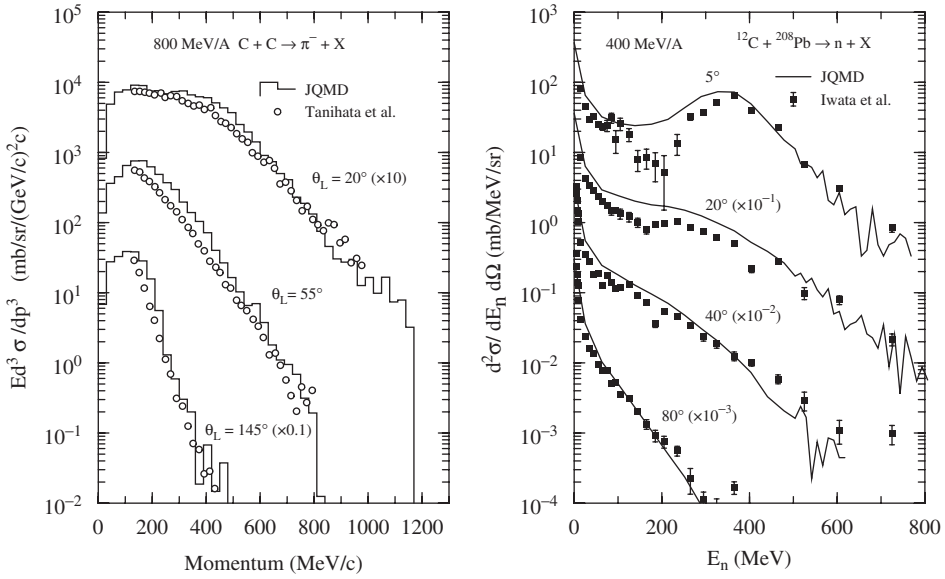

Fig. 5. (a) (left panel) π^- energy spectra for the reaction ^{12}C (800 MeV/u)+^{12}C and (b) (right panel) neutron energy spectra for the reaction ^{12}C (400 MeV/u)+^{208}Pb at different laboratory angles as indicated in the figure. The solid histograms and the solid lines are the results of the JQMD code and the open circles and solid squares denote the experimental data taken from (Tanihata et al., 1979; Iwata et al., 2001). The ordinate of left panel is the Lorentz invariant double differential cross section as a function of the momentum of the emitted pion, while the ordinate of the right panel is the double differential cross section as a function of the neutron energy.

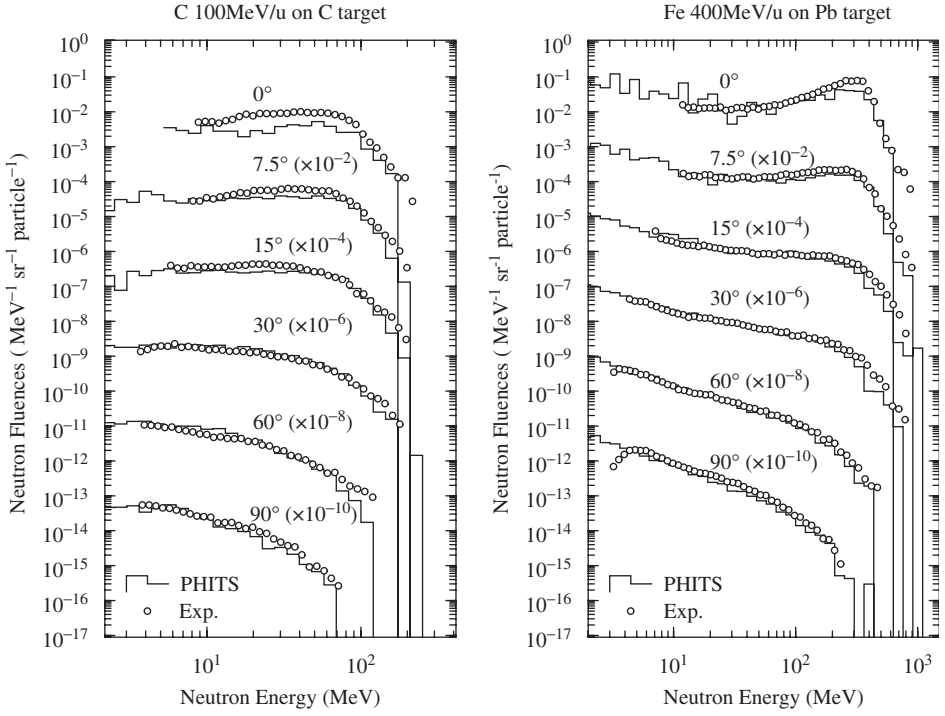

Fig. 6. Comparison of the neutron fluence calculated with PHITS and the measured data for 100 MeV/u C ion on C target (left panel) and 400 MeV/u Fe ion on Pb target (right panel).

reproduced the measured cross sections for the C beams with thin target.

PHITS has incorporated the JQMD code for the collision part of the nucleus–nucleus reactions to describe the secondary neutron yields from the thick target. In order to investigate the accuracy of the PHITS code in the heavy ion transport calculation, we have first compared the results with the experimental data measured by Kurosawa et al. (1999a–c). They measured

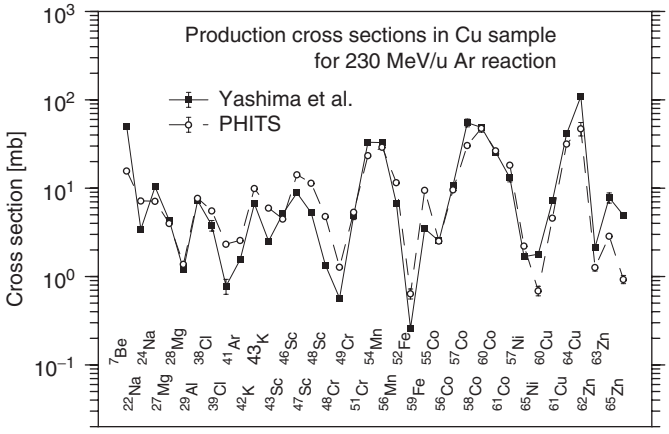

Fig. 7. Comparison of production cross section calculated with PHITS and the measured data for 230 MeV/*u* Ar ion on Cu target.

secondary neutrons produced from thick (stopping length) targets of C, Al, Cu, and Pb bombarded with various heavy ions from He to Xe. Incident energies ranged from 100 to 800 MeV/*u* from HIMAC. Here we show two examples of the comparisons in Fig. 6. It is confirmed from these comparison with measurements that the PHITS code provides good results on the angular distributions of secondary neutron energy spectra produced from thick carbon, aluminum, copper, and lead targets bombarded by 100 MeV/*u* carbon, 400 MeV/*u* carbon, and 400 MeV/*u* iron ions.

Next validation of PHITS is the comparisons of the spallation products induced in a thick target by high energy heavy ions. Yashima et al. (2002, 2003, 2004a,b) systematically measured the residual radioactivities by irradiating Ar(230, 400 MeV/*u*), Si(800 MeV/*u*), Ne(100, 230, 400 MeV/*u*), C(100, 230, 400 MeV/*u*), He(100, 230 MeV/*u*) and p(100, 230 MeV) ions on a Cu target at HIMAC. They have compared the PHITS results with the experimental results of the production cross sections. One of the results for Cu sample of Ar induced reaction at 230 MeV/*u* is shown in Fig. 7. The results of PHITS agree in general with the experimental values within a factor of 2, except for heavy products close to target nuclide and the specific products in the lighter mass region.

3.7. Tally and utilities

User interface and tally, which is a detector in the code to get desirable information from the simulation, are important equipment in a multi-purpose transport code. PHITS provides a variety of tallies to score track length, flux and current of crossing surface, produced particle and residual nucleus at the collision, average heat and distribution of deposit energy, star density, and DPA (displacements per atom). These quantities can be tallied in a cell defined by the geometry and also by the superimposed *r-z* and *xyz* scoring meshes. The meshes of energy, time and angel are additionally set for each tally quantities.

The final results of the tallies are written on a text file. At the same time, PHITS generates an EPS (Enhanced PostScript) file, which can be shown on the monitor as a graph, by the graphic utility ANGEL included in PHITS. This function can be used even in running time of the calculation. So one can check immediately how the calculation proceeds and how the statistics of the tally quantities increases on your monitor in the calculation. This is a good utility in 3D Monte Carlo calculation, since we have to change the parameters of the variance reduction in an iterative way to get good statistics.

4. Application fields of PHITS

PHITS has been used in a wide field of applications from semiconductor soft error up to shielding of spacecrafts. In this section, we introduce three major application fields of PHITS, spallation neutron source, heavy ion therapy, and space radiation.

4.1. Spallation neutron source

J-PARC (The Joint Project Team of JAERI and KEK, 2000) (Japan Proton Accelerator Research Complex) project is a main field where the NMTC/JAM code had been developed. This project has a 400 MeV normal-conducting LINAC, superconducting LINAC from 400 to 600 MeV, 3 GeV synchrotron ring for 1 MW proton, and 50 GeV synchrotron ring for 0.75 MW proton beams. These are now under construction and aim to pursue frontier science in particle physics, nuclear physics, materials science, life sciences and nuclear technology, using a new proton accelerator complex at the highest beam power in the world.

A reliable transport code was required for the shielding design and optimization study of each facility in J-PARC. The condition which should be satisfied in the transport code is very severe, since the energy range is very wide from 50 GeV down to meV neutrons in material science facility. Furthermore, the dimension of the system is very large about several tens of meters, but the resolution of the calculation must be of the order of millimeter. First the NMTC/JAM (Niita et al., 2001) code was developed to satisfy these severe conditions, and then the code was upgraded to PHITS, which also includes heavy ion transport.

Here we show an example of the PHITS calculations for the optimization study of the spallation neutron source. Figs. 8 and 9 show the 3D and 2D representation of the calculation model around the mercury target, which can be plotted by the graphical utility of PHITS from the input data. There are two moderators above the target and one moderator under it surrounding by beryllium and iron reflectors. Fig. 10 is a snapshot of the transport phenomena at 50 ns from the moment when 50 protons go into the target. For longer time after this moment, many low energy neutrons go around and fill almost whole region of the reflectors.

For validation of the PHITS calculations for the neutron flux produced by the mercury target, we have applied PHITS to the experiments under the ASTE (AGS Spallation Target

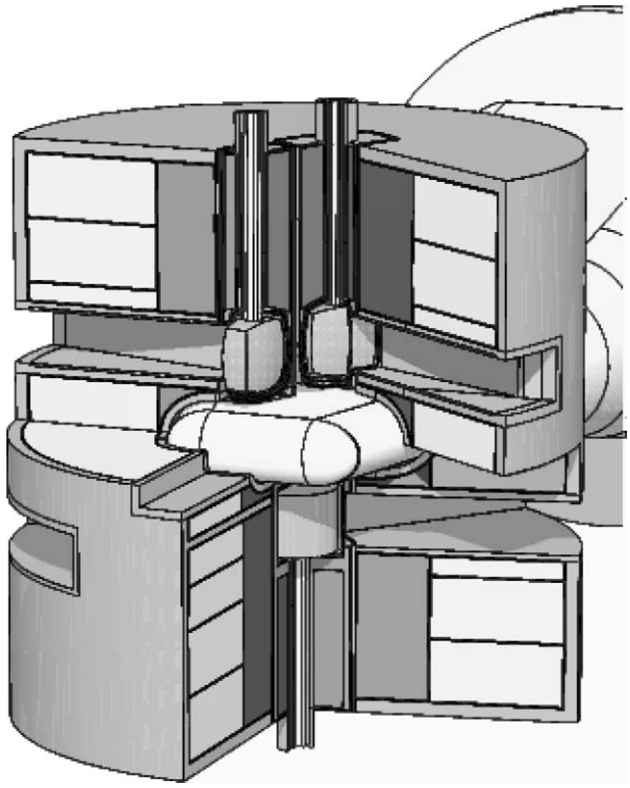

Fig. 8. 3D representation of the calculation model around the mercury target.

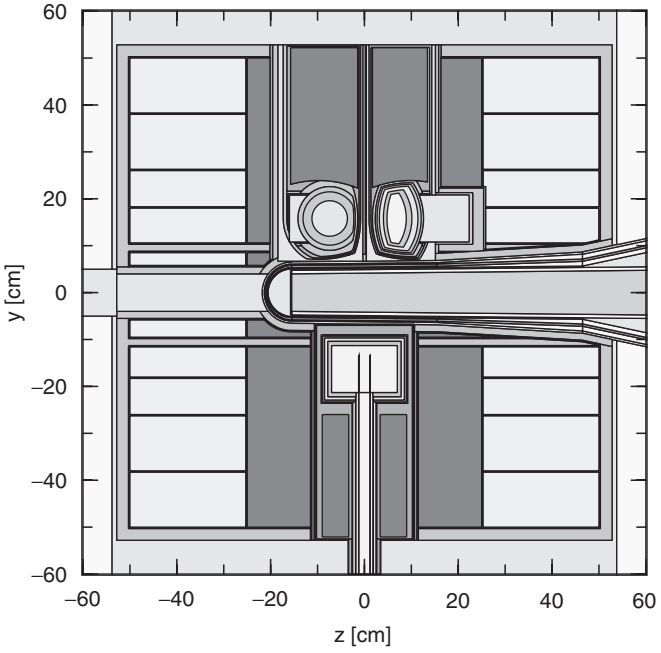

Fig. 9. 2D representation of the calculation model around the mercury target.

Experiment) collaboration (Takada et al., 1998). This experiment was carried out using a thick mercury target, which is a 20 cm diameter and 130 cm long cylinder, and detecting the reaction rate distributions along the cylindrical surface of the target by activation techniques at incident proton energies of 1.6, 12 and 24 GeV. Various activation detectors such as the

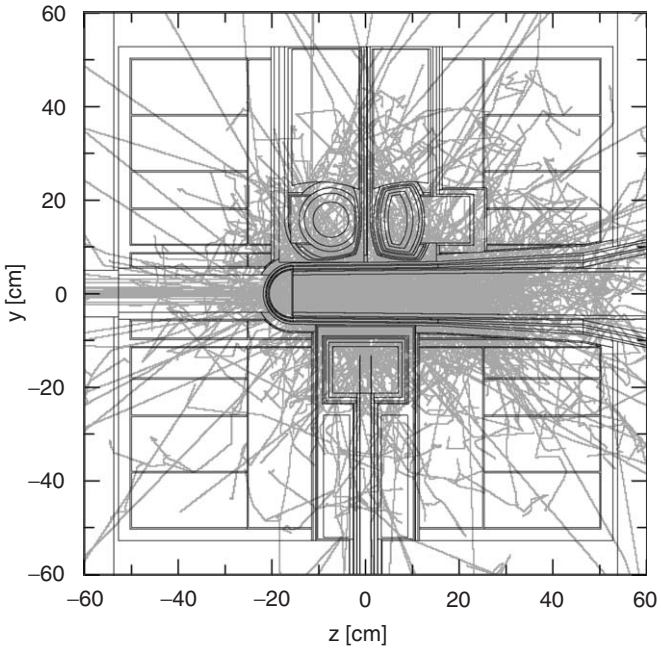

Fig. 10. Snapshot of the transport picture at 50 ns from the moment when 50 protons go into the target.

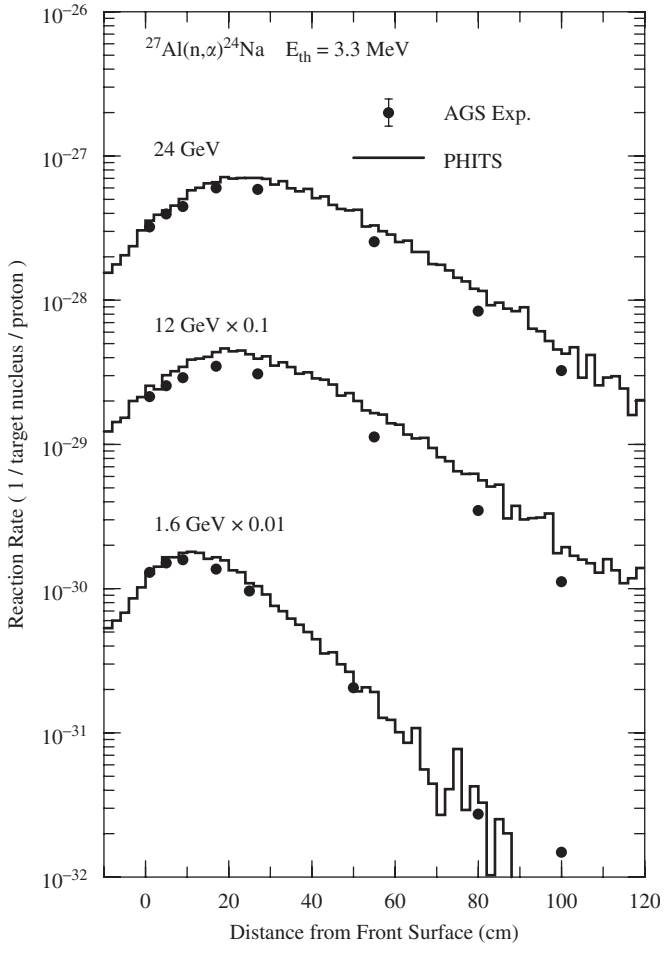

Fig. 11. Distribution of the ^{27}Al(n, α) Na reaction rates along the cylindrical surface of a mercury target bombarded with 1.6, 12 and 24 GeV protons. The solid histograms denote the results of PHITS.

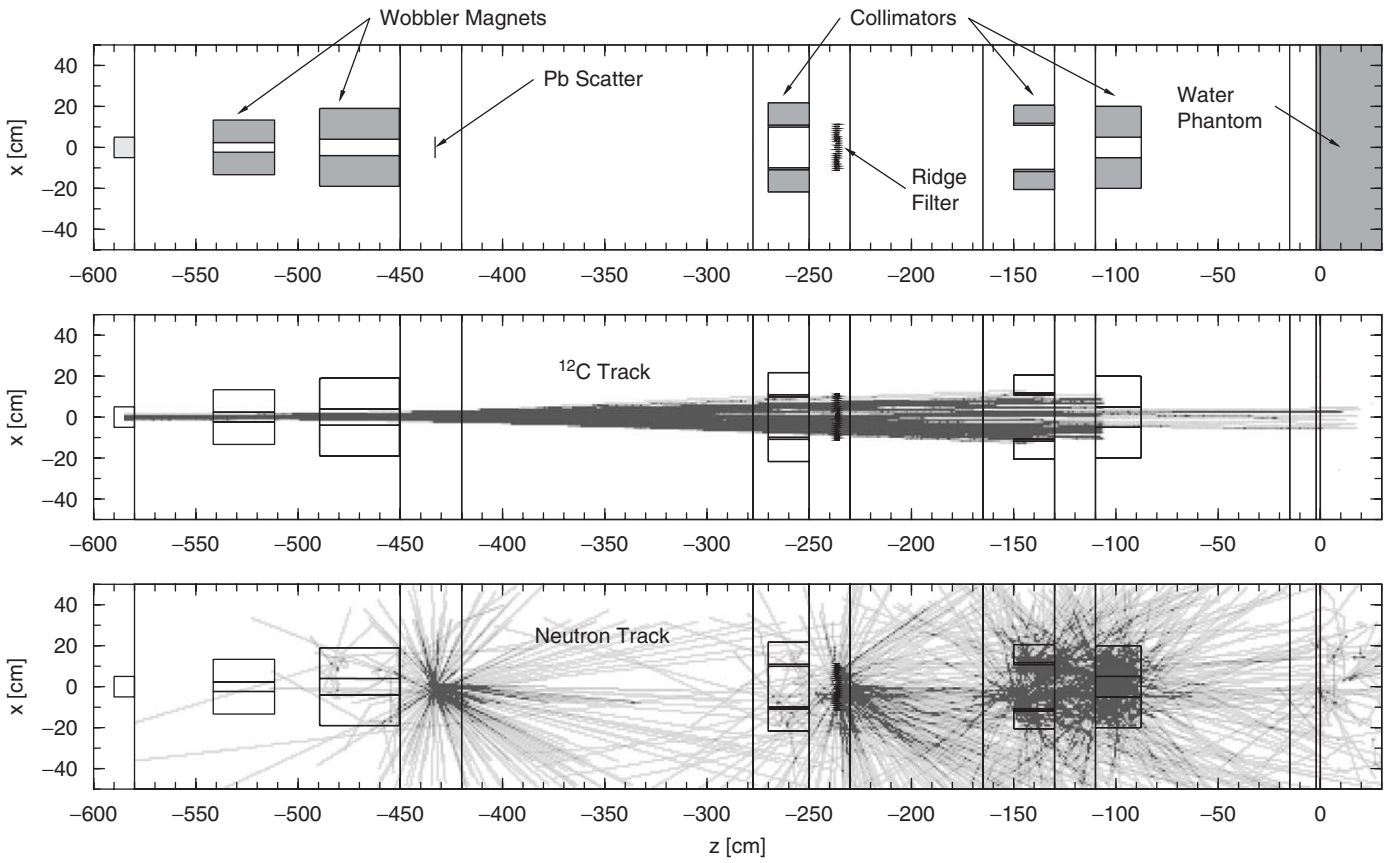

Fig. 12. The calculation setup for ^{12}C with 400 MeV/u beam transport and stopping process in the water phantom (upper panel). The tracks of ^{12}C in the calculation (middle panel). The neutron tracks produced by the collisions (lower panel).

^{115}In$(n, n')^{115m}$In, ^{93}Nb$(n, 2n)^{92m}$Nb and ^{209}Bi(n, xn) reactions with threshold energies ranging from 0.3 to 70.5 MeV were employed to obtain the reaction rate data for estimating spallation source neutron characteristics of the mercury target. Fig. 11 shows the distribution of the ^{27}Al$(n, \alpha)^{24}$Na reaction rates along the cylindrical surface of mercury target bombarded with 1.6, 12, and 24 GeV protons. The threshold of this reaction is 3.3 MeV, while the most effective neutron energy for this reaction is roughly 10 MeV. The results of PHITS, denoted by the solid histograms in these figures, reproduce the experimental distribution quite well for all positions and all energies.

4.2. Heavy ion therapy

Proton and heavy ion therapy is an important field for the development of PHITS, since the accuracy demanded by this field is quite high and the components included in the facilities such as the Wobbler magnet, scatter and ridge filter, which affect the beam profile and then the final dose distributions, should be treated properly by PHITS. We have recently made a comparison of the PHITS results with the experimental data (Nose et al., 2005) measured at HIMAC by simulating the realistic experimental setup. The upper panel of Fig. 12 shows the calculation model of PHITS which consists of two Wobbler magnets for broadening the initial ^{12}C pencil beam, Pb scatter' for smearing the beam, some collimators, and ridge filter for broadening the energy. The ^{12}C beam with 400 MeV/u energy is transported through these components and goes into the water phantom. The tracks of ^{12}C in the calculation are shown in the

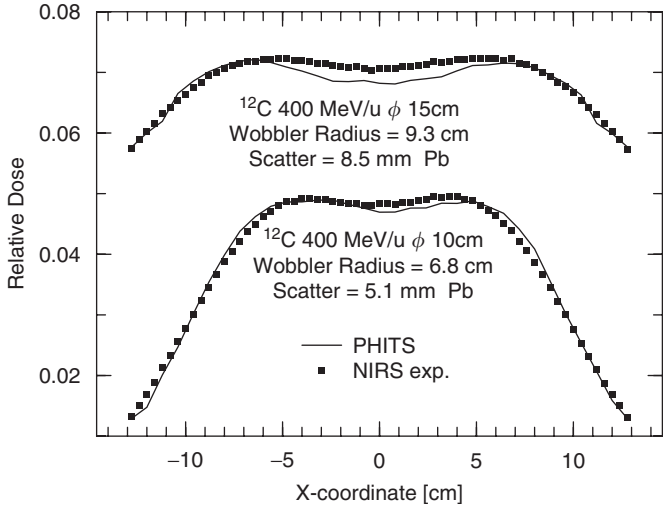

Fig. 13. Transverse distribution of dose at the front surface of the water phantom of all particles through the Wobbler magnets, scatter and collimators without the ridge filter.

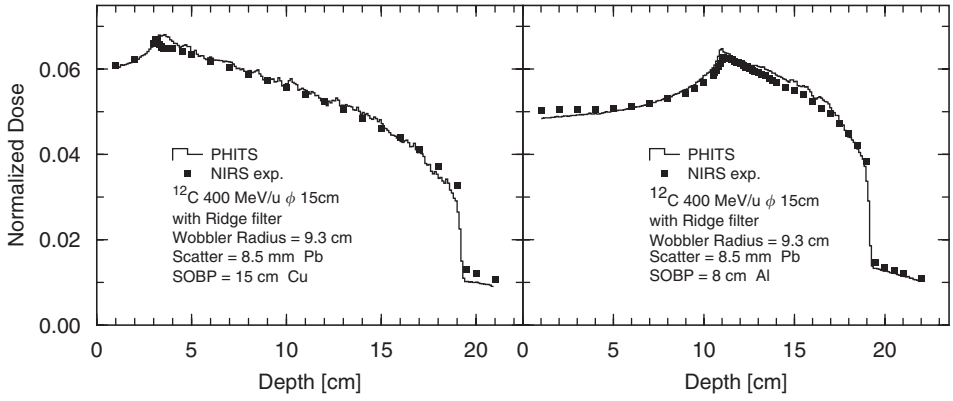

Fig. 14. Dose distribution as a function of the depth of the water phantom. The left and right panel of the figure differ each other for spread out Bragg peak (SOBP) by changing the material and size of the ridge filter indicated in the figure. Since the relative values were measured in the experiments, the values of dose are normalized as the integral values are coincident each other.

middle panel of Fig. 12. In this transport, ^{12}C hits the scatter, ridge filter and collimators. The neutron tracks produced by the collisions are shown in the lower panel of Fig. 12.

Fig. 13 shows the transverse distribution of dose at the front surface of the water phantom of all particles through the Wobbler magnets, scatter and collimators without the ridge filter. The solid squares denote the experimental data measured at HIMAC in NIRS, while the solid lines show the results of PHITS. The upper and lower results are the results with different conditions of the radius of Wobbler spreading and thickness of the scatter indicated in the figure. The results from the PHITS simulation underestimate a little at the center region. However, this tiny deviation affects the dose distribution in the water if the ridge filter is put in. Fig. 14 show the dose distribution as a function of the depth of the water phantom. The left and right panel of the figure differ from each other for SOBP (Spread Out Bragg Peak) by changing the material and size of the ridge filter. The results of PHITS show overall good agreement with the experimental data. In an actual application of the heavy ion therapy, however, even the observed small deviation between simulations and measurements should be removed by further improvements of PHITS. However, it should be noted here that these calculations are performed by the default values of the calculation parameters, i.e. without changing any parameters of PHITS used in the calculations shown above and without any turning of $\mathrm{d}E/\mathrm{d}x$, energy and angel straggling for the specific materials.

4.3. Space radiation

The space radiation problem is a field where PHITS might play an important role, since the radiation fields in spacecrafts consist of high energy protons, heavy ions and locally produced neutrons, and their transport phenomena down to low energy neutrons in a complex geometry can be well described by PHITS as shown above in this paper. In order to examine the applicability of PHITS to the space radiation problem, we have first applied PHITS to a shielding problem of the Space Shuttle.

In a previous publication (Sato et al., this issue) on this issue, we have calculated the neutron and charge particle spectra inside the Space Shuttle. As source particles, we considered almost all kinds of space radiations, the trapped and Galactic Cosmic Ray (GCR) protons, albedo neutrons from the earth atmosphere, and heavy ion with charges up to 28 and energy up to 100 GeV/u. The spectrum of albedo neutrons was also calculated by PHITS simulating the earth atmosphere based on the charge particles spectra outside of the earth. We have compared calculated neutron spectra in the imaginary vessel at the solar minimum with the orbit-averaged data measured by BBND (Bonner Ball Neutron Detector) at STS-89 (Matsumoto et al., 2001). An excellent agreement can be observed between the calculated and experimental results, particularly for neutron energies above 1 MeV which is very important in the evaluation of dose for astronauts.

5. Summary

We have developed the multi-purpose Monte Carlo Particle and Heavy Ion Transport code System PHITS. In PHITS, we have incorporated two important models, JAM and JQMD, to simulate the particle induced nuclear reactions up to 200 GeV and the nucleus–nucleus collisions, respectively.

We have described the details of the two models and showed the validations of these models by comparing simulated results with experimental data. For the applications of PHITS, we have introduced three fields; spallation neutron source, heavy ion therapy and space radiation. The results shown in this paper clearly indicate that PHITS has a great ability of carrying out the radiation transport analysis of almost all particles and heavy ions within a wide energy range.

We are, however, still developing the PHITS code by seeking better parameterizations in the JQMD code, improving the systematics and models used for calculation of the reaction cross sections and $\mathrm{d}E/\mathrm{d}x$, adding routines for calculating elastic scattering of heavy ions, and including radioactivity and burnup processes.

References

Aichelin, J., 1991. Phys. Rep. 202, 233.

Armstrong, T.W., Chandler, K.C., 1973. A Fortran program for computing stopping powers and ranges for muons, charged pions, protons, and heavy ions. ORNL-4869, Oak Ridge National Laboratory.

Briesmeister, J.F., et al., 1997. MCNP general Monte Carlo N-particle transport code. Los Alamos National Laboratory report; LA-12625-M.

Chadwick, M.B., et al., 1999. LA150 documentation of cross sections, heating, and damage. Los Alamos National Laboratory report; LA-UR-99-1222.

Chiba, S., Iwamoto, O., Fukahori, T., Niita, K., Maruyama, T., Iwamoto., A., 1996a. Phys. Rev. C 54, 285.

Chiba, S., Chadwick, M.B, Niita, K., Maruyama, T., Iwamoto. A., 1996b Phys. Rev. C 53 1824.

E802 Collaboration, Abbott, T., et al., 1992. Phys. Rev. D 45, 3906.

Furihata, S., 2000. Nucl. Instrum. Methods B 171, 251.

Halbleib, J.A., et al., 1992. ITS Version 3.0: The integrated TIGER series of coupled electron/photon Monte Carlo transport codes. SAND91-1634.

High Energy Reactions Analysis Group, 1983. CERN Report CERN-HERA 83-01 and 83-02 (unpublished).

Iwase, H., Niita, K., Nakamura, T., 2002. J. Nucl. Sci. Technol. 39, 1142.

Iwata, Y., et al., 2001. Phys. Rev. C 64, 054609.

The Joint Project Team of JAERI and KEK, 2000. The Joint Project for High Intensity Proton Accelerators, JAERI-Tech, 2000-003, JAERI.

Kurosawa, T., et al., 1999a. Nucl. Sci. Eng. 132, 30.

Kurosawa, T., et al., 1999b. J. Nucl. Sci. Technol. 361, 42.

Kurosawa, T., et al., 1999c. Nucl. Instrum. Methods A 430, 400.

Kurosawa, T., et al., 2000. Phys. Rev. C 62, 044615.

Matsufuji, N., Fukumura, A., Komori, M., Kanai, T., Kohno, T., 2003. Phys. Med. Biol. 48, 1605.

Matsumoto, H., Goka, T., koga, K., Iwai, S., Uehara, T., Sato, O., Takagi, S., 2001. Radiat. Meas. 33, 321.

McLane, V., et al., 1996. ENDF/B-VI Summary Documentation. BNL-NCS-17541.

Nara, Y., Otuka, N., Ohnishi, A., Niita, K., Chiba, S., 2000. Phys. Rev. C 61, 024901.

NEA Data Bank. Nuclear Data Services: Experimental Data.

Niita, K., Chiba, S., Maruyama, T., Takada, H., Fukahori, T., Nakahara, Y., Iwamoto, A., 1995. Phys. Rev. C 52, 2620.

Niita, K., Takada, H., Meigo, S., Ikeda, Y., 2001. Nucl. Instrum. Methods B 184, 406.

Nose, H., Niita, K., Hara, M., Uematsu, K., Azumi, O., Miyauchi, Y., Komori, M., Kanai, T., 2005. J. Nucl. Sci. Technol. 42, 250.

Particle-Data-Group, 2002. Phys. Rev. D 66, 010001.

Pearlstein, S., 1972. Nucl. Sci. Eng. 49, 162.

Pearlstein, S., 1987. Nucl. Sci. Eng. 95, 116.

Pearlstein, S., 1989. J. Astrophys. Nucl. Sci. Eng. 346, 1049.

Sato, T., Niita, K., Iwase, H., Nakashima, H., Yamaguchi, Y., Sihver, L., this issue. Applicability of Particle and Heavy Ion Transport Code PHITS to the Shielding Design of Spacecraft.

Shibata, K., et al., 2002. Japanese evaluated nuclear data library version 3 revision-3: JENDLE-3.3. J. Nucl. Sci. Technol. 39, 1125.

Sihver, L., Schardt, D., Kanai, T., 1998. Jpn. J. Med. Phys. 18, 1.

Sjöstrand, T., 1994. Comp. Phys. Comm. 82, 74.

Takada H., et al., 1998. Measurements of reaction rate distributions on a mercury target bombarded with high energy protons, Proceedings of the 14th Meeting of the International Collaboration on Advanced Neutron Sources, Illinois, 1998, vol. II, ANL-98-33, Argonne National Laboratory, USA.

Tanihata, I., et al., 1979. Phys. Lett. B 87, 349.

Tripathi, R.K., Cucinotta, F.A., Wilson, J.W., 1996. Nucl. Instrum. Methods B 117, 347.

Tripathi, R.K., Wilson, J.W., Cucinotta, F.A., 1997. Nucl. Instrum. Methods B 129, 11.

Tripathi, R.K., Cucinotta, F.A., Wilson, J.W., 1999. Nucl. Instrum. Methods B 155, 349.

Wang, X.N., Gyulassy, M., 1991. Phys. Rev. D 44, 3501.

Wang, X.N., 1997. Phys. Rep. 280, 287.

Wang, X.N., Gyulassy, M., 1994. Comp. Phys. Comm. 83, 307.

Wen-quinf, S., Bing, W., Jun, F., Wen-logn, Z., Yong-tai, Z., En-pu, F., 1989. Nucl. Phys. A 491, 130.

Wilson, J.W., Chun, S.Y., Badavi, F.F., Townsend, L.W., Lamkin, S.L., 1991. HZETRN: A heavy ion and nucleon transport code for space radiations. NASA TP-3146, NASA Langley Research Center, Hampton, VA.

Yashima, H., et al., 2002. Phys. Rev. C 66, 044607.

Yashima, H., et al., 2003. Radiochim. Acta 91, 689.

Yashima, H., et al., 2004a. Nucl. Instrum. Methods B 226, 243.

Yashima, H., et al., 2004b. Radiat. Prot. Dosim. 112, 195.